Reflection Soliton Oscillator

O. Ozgur Yildirim, *Student Member, IEEE*, David S. Ricketts, *Member, IEEE*, and Donhee Ham, *Member, IEEE*

***Abstract*—We report on an electrical oscillator that self-generates a periodic train of short-duration pulses. The oscillator consists of a nonlinear transmission line (NLTL), one end of which is connected to a one-port amplifier and the other end is open. In the steady state, a self-generated short-duration pulse travels back and forth on the NLTL, reflected at both ends of the NLTL due to impedance mismatches. The one-port amplifier produces a negative output resistance for a voltage beyond a particular threshold and a positive output resistance for a voltage below that threshold, and thus, the reflection from the amplifier provides gain for the main upper portion of the pulse to compensate loss, and attenuates small perturbations to ensure oscillation stability. The NLTL substantially sharpens the pulse.**

***Index Terms*—Electrical solitons, mode-locked oscillators, nonlinear transmission lines (NLTLs), oscillators, pulse oscillators, solitons.**

I. Introduction

ELECTRICAL oscillators that can generate a periodic train of short-duration pulses can be useful in a number of applications, including high speed sampling, time domain reflectometry, ultra wideband radars, and high power RF generation [1]–[3]. A few different types of such pulse oscillators have been developed [see Fig. 1(a)–(c)] [4]–[7]. In this paper, we introduce a new type of pulse oscillator [see Fig. 1(d)].

In 1955, Cutler arranged an amplifier and a linear transmission line in a circular topology [see Fig. 1(a)], which self-generated a stable periodic train of short-duration pulses [4]. The amplifier provides gain for a signal beyond a certain threshold, and attenuates a signal below that threshold. This *level-dependent gain* is the key to the stable pulse oscillation.[1] More specifically: first, the level-dependent gain sharpens the amplifier's input signal, enabling pulse formation; second, the level-dependent gain, especially the attenuation below the threshold, suppresses small perturbations (e.g., noise, reflection) that could grow into undesired pulses and disrupt a stable pulse oscillation. In the steady state, a pulse circulates in the loop. The transmission line is to introduce a delay between one pulse event and the next at any point in the loop.

Manuscript received December 22, 2008; revised May 25, 2009. First published August 25, 2009; current version published October 14, 2009. This work was supported by the Army Research Office under Grant W911NF-06-1-0290.

O. O. Yildirim and D. Ham are with the School of Engineering and Applied Sciences, Harvard University, Cambridge, MA 02138 USA (e-mail: yildirim@fas.harvard.edu; donhee@seas.harvard.edu).

D. S. Ricketts is with the Electrical and Computer Engineering Department, Carnegie Mellon University, Pittsburgh, PA 15232 USA (e-mail: ricketts@ece.cmu.edu).

Color versions of one or more of the figures in this paper are available online at http://ieeexplore.ieee.org.

Digital Object Identifier 10.1109/TMTT.2009.2029025

[1]The level-dependent gain concept was adopted in optics for short-duration light pulse generation, helping pave the way for the field of mode-locked laser. In optics, the level-dependent gain is called *saturable absorption*.

In 1978, Haus *et al.* altered Cutler's oscillator into the form of Fig. 1(b) [5]. Instead of circulating a pulse, a pulse is made travel back and forth on a transmission line[2,3] through reflection at both ends of the line. Like in Cutler's oscillator, level-dependent gain is needed for pulse formation and oscillation stabilization. It is realized as a combination of a constant gain (which occurs in reflection at one line end terminated with an approximately constant negative resistance) and a level-dependent attenuation (which occurs in reflection at the other line end terminated with a level-dependent positive resistance).

In Cutler and Haus's oscillators, the transmission line serves as a simple pulse propagation medium. An interesting design alteration to obtain much sharper pulses would be to incorporate a pulse-sharpening mechanism into the line, in addition to the pulse sharpening provided by the level-dependent gain. Recently, in [6] and [7], some of the authors of this paper indeed developed such an oscillator [see Fig. 1(c)]. By replacing, in Cutler's circular topology, a linear transmission line with a *nonlinear transmission line* (NLTL) [a transmission line periodically loaded with varactors (nonlinear capacitors)], which had been long known for its superb pulse sharpening capability [8]–[12], we attained a circuit that robustly self-generated a stable, periodic train of much sharper pulses. The sharp pulses on the NLTL, which possess unique nonlinear properties, are known as *solitons* [8]–[14]. Thus, we called the oscillator *electrical soliton oscillator*.

Solitons circulating in the oscillatory loop exhibit rich nonlinear dynamics, and unless suitably controlled, they tend to form a soliton pulse train with significant variations in the pulse amplitude and repetition rate. The key to our success in overcoming this oscillation instability and building the soliton oscillator of Fig. 1(c), [6], [7] that robustly self-generated a train of solitons with constant soliton amplitude and repetition rate was to realize that the level-dependent gain used for pulse sharpening and oscillation stabilization in Cutler's oscillator is also effective in stabilizing the soliton oscillation. However, since the soliton oscillator has a much stronger tendency towards instability due to soliton's nonlinear dynamics, its stabilization demanded more from the amplifier's level-dependent gain. In the soliton oscillator, the dominant pulse sharpening mechanism is provided not by the level-dependent gain, but by the NLTL.

If the circular soliton oscillator [see Fig. 1(c)] is an extension from Cutler's oscillator [see Fig. 1(a)] to obtain sharper pulses, can an analogous design extension be made from Haus's reflection oscillator [see Fig. 1(b)] to obtain sharper pulses?

[2]Although Haus *et al.* used a metallic waveguide, we may think of it as a transmission line, as both have the same goal of introducing a delay.

[3]The actual pulse in Haus's oscillator is not the baseband pulse shown in Fig. 1(b), but a pulse with a sinusoidal modulation. The essence of Haus's work, however, lies in the generation of the pulse envelope, as described here.

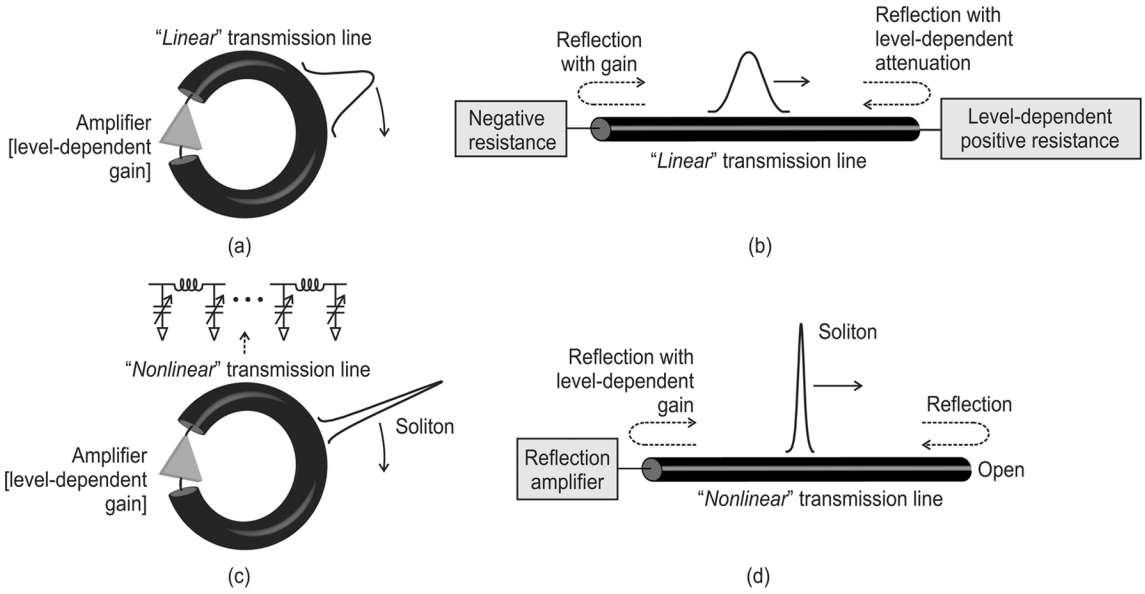

Fig. 1. (a) Cutler's circular linear pulse oscillator [4]. (b) Haus's reflection linear pulse oscillator [5]. (c) Our circular soliton pulse oscillator [6], [7]. (d) Our reflection soliton pulse oscillator (this work).

This paper reports on such a *reflection soliton oscillator* [see Fig. 1(d)]. This work starts by replacing the linear transmission line in Haus's oscillator with an NLTL to establish a dominant pulse sharpening mechanism in the pulse propagation medium. The level-dependent gain needed for soliton oscillation stability [6], [7] is incorporated in a single one-port amplifier connected to one end of the NLTL: it produces a negative resistance for a voltage beyond a certain threshold and a positive resistance for a voltage below that threshold, and thus, the reflection from the amplifier end provides gain for the main upper portion of a pulse to compensate loss, while attenuating small perturbations. The other end of the NLTL is open for reflection. In Haus's oscillator where pulse sharpening is achieved solely through the level-dependent gain, the pulse sharpening is limited by the bandwidth of the active circuit providing the level-dependent gain. In contrast, our reflection soliton oscillator, where the pulse sharpening executed dominantly by the NLTL is not limited by the amplifier bandwidth, achieves substantially more pulse sharpening.

In Section II, we present the operating principle of our reflection soliton oscillator. Section III describes the design of the one-port amplifier that executes the level-dependent gain function. Section IV reports on experimental results. In Section V, we experimentally compare our oscillator and Haus's oscillator we recreated. Section VI compares reflection and circular soliton oscillators.

II. Reflection Soliton Oscillator—Operating Principle

Our reflection soliton oscillator consists of an NLTL terminated with a one-port amplifier at one end and an electrical open at the other end (see Figs. 1(d) or 2). In the steady state (we will address oscillation startup in Section III), a pulse travels back and forth on the NLTL (see Fig. 2). The pulse reflected at the amplifier end travels down the NLTL towards the open, during which the NLTL compresses the pulse, forming it into a sharp soliton. As the soliton reaches the open, it is reflected to travel back towards the amplifier, during which the soliton lowers amplitude and broadens width in a particular manner [15] due to loss in the NLTL. Once the damped soliton reaches the amplifier, a reflection with level-dependent gain occurs, which compensates loss and reinforces oscillation stability. The reflected pulse is not a soliton, as the amplifier deforms the soliton shape. The reflected reenergized pulse repeats the spatial dynamics described above, again forming into a soliton as it propagates down the NLTL toward the open.

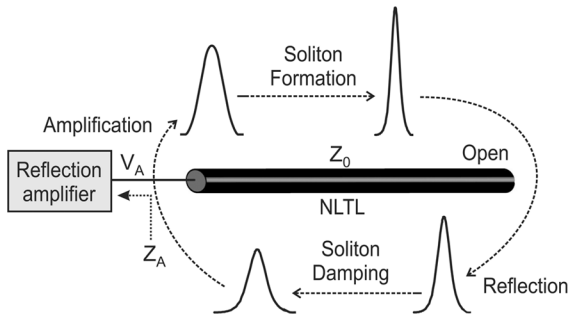

Fig. 2. Steady-state dynamics in our reflection soliton oscillator.

A. Reflection at the Amplifier End

The reflection with level-dependent gain at the amplifier end is achieved as follows. The output impedance of the amplifier Z_A seen by the NLTL, is a function of voltage V_A at that output node. If we denote the average characteristic impedance[4] of the

[4]The NLTL's characteristic impedance at a given point varies with the voltage applied to the varactor at that point due to the voltage dependence of the varactor capacitance. Here, we take the average characteristic impedance seen by a signal to capture the essence in a simple, albeit not the most accurate, manner.

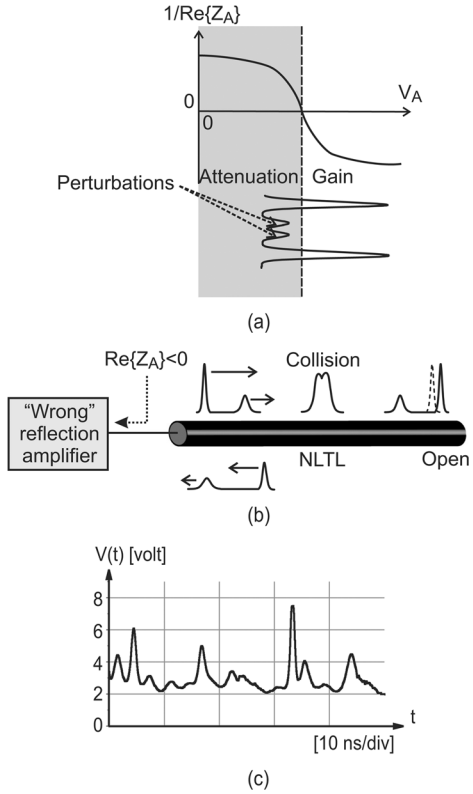

Fig. 3. Soliton oscillation stability consideration. (a) Hypothetical depiction of the desired $\mathrm{Re}\{Z_A\}$ versus V_A to yield level-dependent gain. (b) Buildup of soliton oscillation instability when gain is provided for all signal levels. (c) Measured unstable oscillation when gain is provided for all signal levels.

NLTL as Z_0, the reflection coefficient Γ at the amplifier end with a voltage of V_A is given by

$$\Gamma(V_A) = \frac{Z_A(V_A) - Z_0}{Z_A(V_A) + Z_0}. \tag{1}$$

Since $Z_0 > 0$, we see that

$$|\Gamma(V_A)| \begin{cases} > 1 \text{ (gain)}, & \text{if } \mathrm{Re}\{Z_A(V_A)\} < 0 \\ < 1 \text{ (attenuation)}, & \text{if } \mathrm{Re}\{Z_A(V_A)\} > 0. \end{cases} \tag{2}$$

Therefore, for the amplifier to provide a gain for a voltage larger than a certain threshold and to attenuate a signal smaller than the threshold, we are to have $\mathrm{Re}\{Z_A\} < 0$ for V_A above the threshold, and $\mathrm{Re}\{Z_A\} > 0$ for V_A below the threshold, as hypothetically drawn in Fig. 3(a). This is how the reflection with level-dependent gain is attained. We will detail the design of such an amplifier in Section III.

Let us examine what would happen if the level-dependent gain is not in force, or more specifically, if $\mathrm{Re}\{Z_A\} < 0$ regardless of V_A, and all signal levels receive gain upon reflection from the amplifier end. Suppose a desired soliton pulse and a small parasitic soliton pulse produced by a perturbation (e.g., noise) in the oscillator [see Fig. 3(b)]. Both of these pulses will be reflected with gain at the amplifier end, and the parasitic pulse will persist, as the amplifier in this scenario does not attenuate low-level signals. Since the two reflected pulses have different amplitudes, they propagate at different velocities (a taller pulse propagates faster than a shorter pulse—this is a key soliton property [6], [7]), thus eventually colliding with each other. This collision, which is a nonlinear process, causes pulse amplitude modulation at the moment of collision (see Fig. 3(b), middle), and pulse position modulation after the collision (see Fig. 3(b), right—the taller pulse would appear as the dashed one in the different position, were it not for the collision), which is another key soliton property [6], [7]. Therefore, the pulse train produced with gain at all signal levels exhibits significant variations in pulse amplitude and repetition rate. See Fig. 3(c) for an unstable oscillation observed in one of our actual prototypes. In contrast, when level-dependent gain is in force, small perturbation falls in the attenuation region to be suppressed [see Fig. 3(a)], no soliton collision occurs, and the instability is prevented.

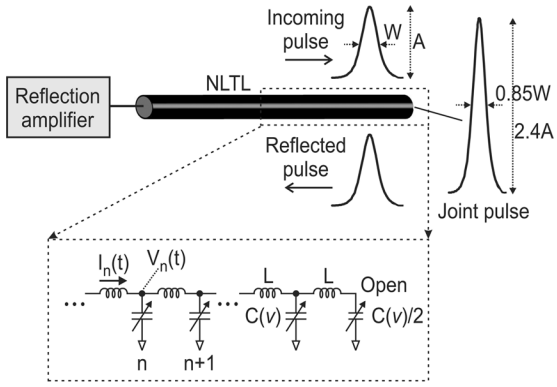

Fig. 4. Reflection at the open end of the NLTL.

B. Reflection at the Open End

The pulse reflection at the open end of the NLTL, illustrated in Fig. 4, is interesting and useful, as it offers an extra pulse-sharpening mechanism, in addition to the sharpening that occurs during pulse propagation on the NLTL.

At the open end, the incoming pulse is reflected into a same shape pulse. The incoming and reflected pulses (voltages) superpose to increase the joint voltage at the open end. If a linear line is used, the joint voltage at the open end is twice the incoming voltage. In case of the NLTL, the joint voltage is *larger* than twice the incoming voltage. This is due to the voltage dependence of the capacitance of the varactor at the open end. The superposed (thus increased) voltage reduces the capacitance, and to conserve the total energy despite the reduced capacitance, the superposed voltage should be larger than twice the incoming voltage [9]. In our measurement [see Section IV], the joint voltage amplitude is 2.4 times larger than the incoming voltage in amplitude.

This pulse amplification at the open end by a factor larger than two translates to pulse sharpening. In an NLTL constructed in the form of a ladder network of inductor–varactor sections (see Fig. 4), the time integration of an arbitrary pulse voltage $V_n(t)$ at the nth node is constant, independent of the position n [9] (see Appendix A):

$$\int_{-\infty}^{\infty} V_n(t)dt = \text{constant}. \tag{3}$$

In other words, if one measures the area under the time-domain voltage waveform $V_n(t)$, the area will remain the same, independently of n. Therefore, the time-domain area of the joint

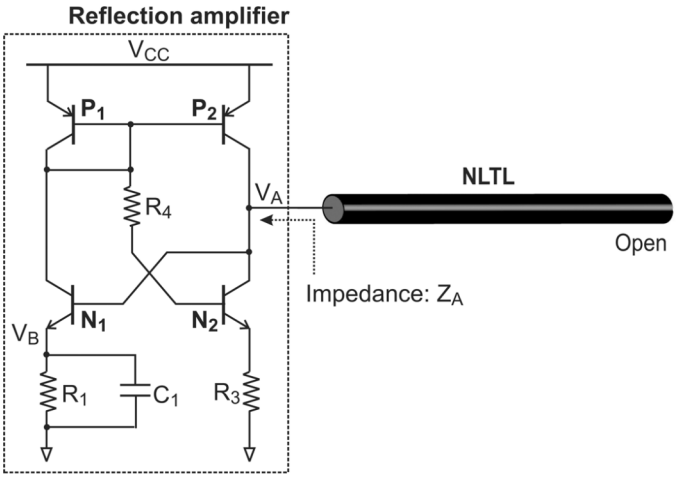

Fig. 5. Our one-port reflection amplifier.

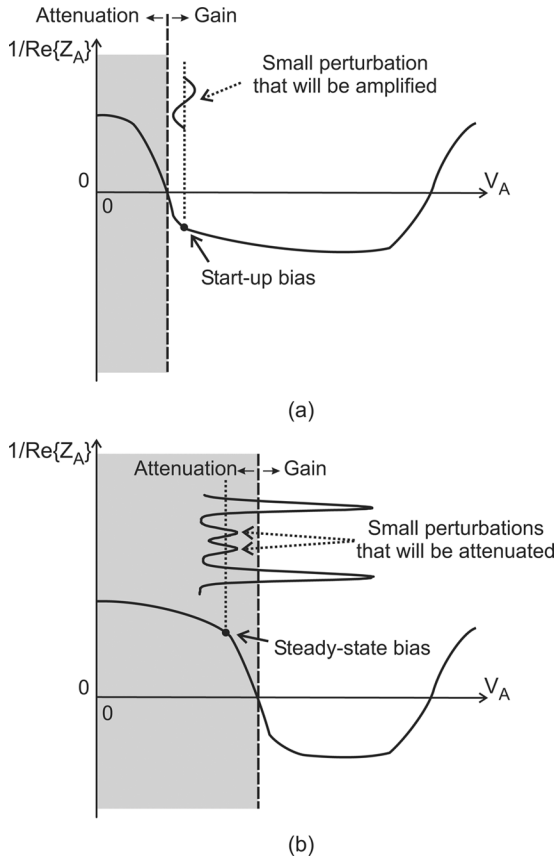

Fig. 6. $1/\mathrm{Re}\{Z_A\}$ versus V_A. (a) Initial startup stage. (b) Steady state.

voltage pulse at the open end should be twice the time-domain area of the incoming voltage pulse, whose amplitude is A and temporal width is W. Since the time-domain area of a pulse may be approximated as a product of its amplitude and temporal width, the time-domain area of the joint voltage pulse is $2AW$. Therefore, the amplitude $2.4A$ of the joint pulse corresponds to the temporal width of $0.83W$ (in our experiment of Section IV, the measured width is $0.85W$). Thus, the joint pulsewidth $0.83W$ at the open end is smaller than the incoming pulsewidth W.

III. Reflection Soliton Oscillator—Amplifier Design

A. Need for an Adaptive Bias Scheme

As discussed in Section II, the reflection amplifier in Fig. 2 should be capable of level-dependent amplification such that small perturbations are rejected to ensure oscillation stability, while the main portion of the soliton is amplified to compensate loss. An important notion is that this level-dependent gain is what is required in the *steady state*. In contrast, in the *initial startup transient*, the level-dependent gain should be actually avoided, as small perturbations should be amplified to enable oscillation startup.

To achieve these two contradicting gain characteristics in the same amplifier, an adaptive bias scheme can be employed to shift the gain characteristic of the amplifier from full gain to level-dependent gain as the oscillation grows from an initial transient into a steady-state pulse train. Such an adaptive bias scheme has been actually implemented in various forms in all of the previous pulse oscillators discussed earlier [4]–[7]. In this study, we have also devised an adaptive bias scheme suitable for the reflection soliton oscillator, which we will now explain.

B. One-Port Reflection Amplifier With an Adaptive Bias

Fig. 5 shows our one-port reflection amplifier, which achieves, through an adaptive bias scheme, the full gain during the initial startup transient and the level-dependent gain during the steady state. The basic circuit arrangement is two inverters put back to back: transistors $\mathbf{N}_1$ and $\mathbf{P}_1$ form one inverter; transistors $\mathbf{N}_2$ and $\mathbf{P}_2$ form the other inverter. The underlying design idea is that the real part of the output impedance of the amplifier, $\mathrm{Re}\{Z_A\}$, seen by the NLTL, can assume positive or negative values, depending on the ON/OFF status of $\mathbf{N}_1$, i.e., depending on the voltage difference between V_A and V_B. If $\mathbf{N}_1$ is ON with $V_A > V_B$, the back-to-back inverters are in force and a positive feedback is set up, yielding $\mathrm{Re}\{Z_A\} < 0$. If $\mathbf{N}_1$ is OFF with $V_A < V_B$, the back-to-back inverters do not work, leading to $\mathrm{Re}\{Z_A\} > 0$.

In the beginning of the startup transient, V_A and V_B assume certain initial bias values. The amplifier is arranged in such a way that in this initial stage $V_A > V_B$ and $\mathbf{N}_1$ is ON, thus ensuring $\mathrm{Re}\{Z_A\} < 0$ and enabling an oscillation startup. Fig. 6(a) shows the real part of the simulated small-signal impedance Z_A at various dc voltages V_A applied at the output of the amplifier. As can be seen, the initial V_A bias sits in the gain region where $\mathrm{Re}\{Z_A\} < 0$, and thus a small perturbation around the bias receives gain to grow into a pulse train.

As the oscillation grows, a train of pulses starts appearing at the output node of the amplifier. See Fig. 7 in conjunction with Fig. 5 for the following description. When a pulse arrives at the amplifier from the NLTL, V_A goes up. Following V_A, the emitter voltage V_B of $\mathbf{N}_1$ is increased, charging capacitor C_1. Due to $\mathbf{N}_1$, the time constant associated with this charging of C_1 is much smaller than R_1C_1, the time constant of the R_1–C_1

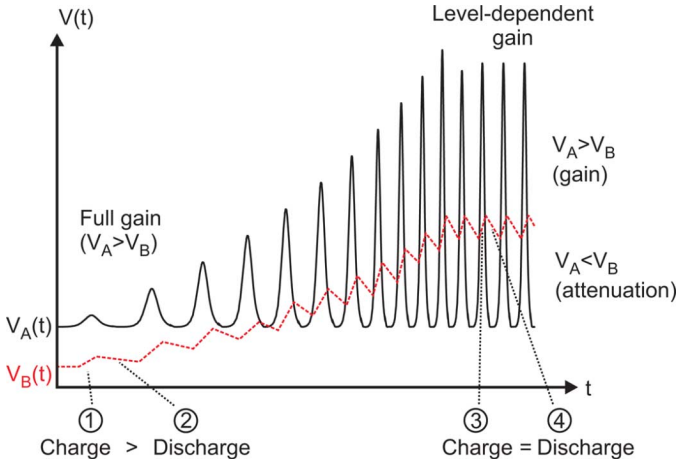

Fig. 7. Illustration of a startup transient into steady state.

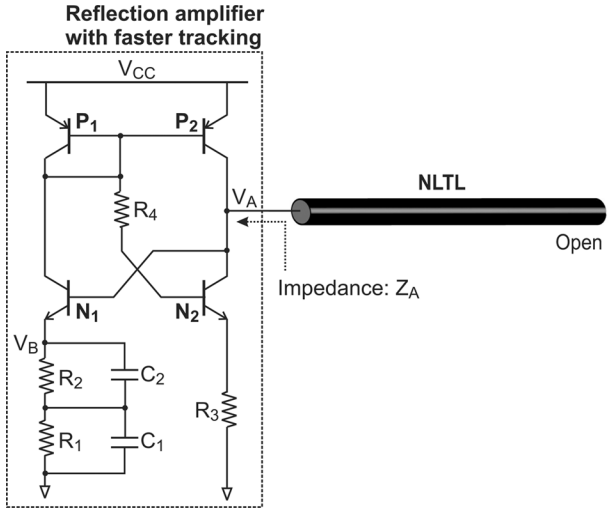

Fig. 8. Our reflection amplifier with an improved R–C network.

network.[5] Now as the pulse leaves the amplifier and V_A is decreased, $\mathbf{N}_1$ is turned off because V_B is still high, and the charge stored on C_1 starts being discharged through the R_1–C_1 network with a time constant of R_1C_1: the discharging of C_1 in the absence of a pulse is slower than its charging in the presence of a pulse. We set the value of R_1C_1 larger than the pulse repetition period so that by the time the next pulse arrives, the discharging has not been sufficient to empty what was charged during the previous pulse event (see ① and ②, Fig. 7), and thus, V_B has been increased overall (see Fig. 7). As this process is repeated with continued arrivals and departures of pulses, the overall charges in C_1 are increased at every pulse event, and the dc average (bias) of V_B goes up. In this way, once the steady state is reached (we will explain shortly how the dc average of V_B eventually settles to a constant value), the bias of V_B assumes a value larger than that during the initial startup.

Due to this increased V_B, in the steady state, turning on $\mathbf{N}_1$ to generate a negative $\mathrm{Re}\{Z_A\}$ and to produce gain requires a higher level of voltage at V_A (see Fig. 7). This corresponds to the fact that in the steady state, the $1/\mathrm{Re}\{Z_A\}$ versus V_A curve is shifted to the right, as hypothetically shown in Fig. 6(b): negative $\mathrm{Re}\{Z_A\}$, or gain, is attainable at higher voltages. The steady-state bias (dc average) of V_A has been shifted to the right as well due to the increased pulse height, but this shift is not as large as the shift in the impedance curve, and thus, the steady-state bias lies in the attenuation region. Overall, the steady-state pulses lie across the attenuation and gain regions, as shown in Figs. 6(b) or 7, and only the higher portion of the pulses will be amplified, while their lower portion and any small undesired perturbations will be suppressed: the level-dependent gain has thus been set up in the steady state.

Shortly before, we asserted that the increase in the dc average of V_B during the initial startup transient eventually settles down to a constant value, which we will explain now. During the very initial transient, the C_1 charging is faster than the C_1 discharging due to the strong action of $\mathbf{N}_1$ that is ON during the pulse event, thus causing the increase in V_B. As the steady state is approached, $\mathbf{N}_1$ turns on during the higher portion of a pulse, but turns off during the lower portion of the pulse, and thus, the effect of $\mathbf{N}_1$, which is not always ON even during the pulse event, has become weaker, and thus, the C_1 charging is not as fast. Due to this slowing down in the C_1 charging rate, at a certain point, the charging during the pulse event and the discharging during the absence of the pulse balance each other out (see ③ and ④, Fig. 7), thus causing the dc average of V_B to settle at a constant value.[6]

From the foregoing description, it is clear that R_1C_1 should be larger than the pulse repetition period T_0 to ensure a slow discharging between two adjacent pulse events so that V_B can grow during the initial startup. In our case, $R_1C_1 \approx 1.7T_0$. Note, however, that too large a value of R_1C_1 should be avoided, as it causes Q-switching oscillation [5], [16].

C. Improved R–C Network

In the initial transient, it is common to see two competing large pulses that appear successively well within the intended pulse repetition period. The amplifier should be able to select only one of them, while eliminating the other, so that the oscillator can eventually produce a periodic train of soliton pulses with a constant amplitude and a constant pulse repetition rate. Consider two such pulses. If the increase in V_B during the first pulse is not fast enough, V_B is still low for the second pulse, and thus, the second pulse receives a large enough gain to be undesirably sustained. To prevent this, V_B should rise fast enough during the first pulse so that by the time the second pulse arrives, V_B is high enough to introduce enough loss for the second pulse to eliminate it. To this end, we introduced an R_2–C_2 network in series with the original R_1–C_1 network, as shown in Fig. 8, with $R_2C_2 \approx 0.06R_1C_1$. This extra R–C network allows for V_B to track V_A fast for the first pulse so that the second pulse can be suppressed.

[5]In the small-signal analysis, the time constant associated with the C_1 charging can be approximated as $R_1C_1/(1 + g_mR_1)$ where g_m is the transconductance of $\mathbf{N}_1$. The charging time constant is smaller than R_1C_1 by a factor of $1 + g_mR_1$. In our large-signal scenario, although the equation above is not exactly the charging time constant, it is a sufficient indication that the charging time constant is smaller than R_1C_1.

[6]The charging rate is still larger than the discharging rate, but the charging time is smaller than the discharging time due to the small duty cycle of the pulse train.

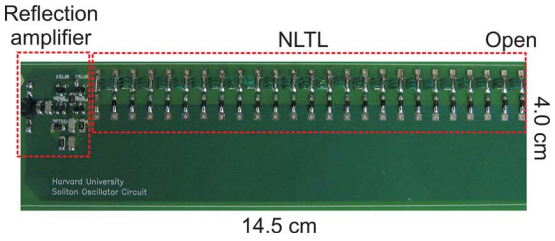

Fig. 9. Reflection soliton oscillator discrete prototype.

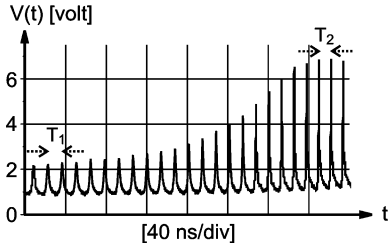

Fig. 10. Measured initial startup transient at the open end of the NLTL.

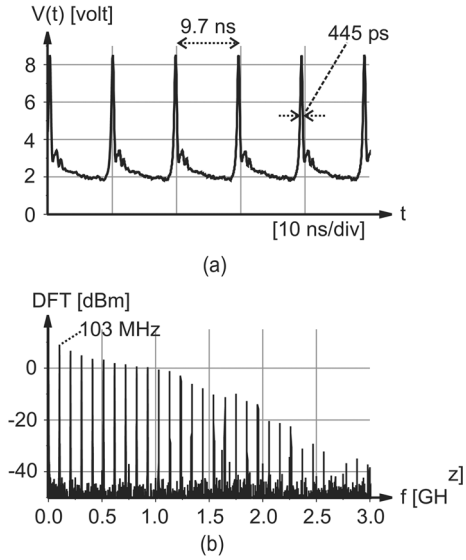

Fig. 11. (a) Measured steady-state oscillation at the open end of the NLTL. (b) Fourier transform of the steady-state waveform.

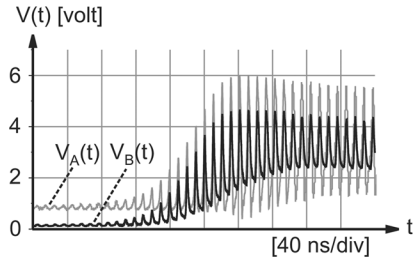

Fig. 12. Measured $V_A(t)$ and $V_B(t)$ from the startup to the steady state.

IV. Experiments

For proof of concept, we constructed a reflection soliton oscillator prototype in a discrete form (see Fig. 9), whose output signal lies across a lower end of the microwave spectral region. The relatively low frequencies were chosen to allow direct probing of the oscillator dynamics using a real-time oscilloscope, and thus to facilitate full verification of the operating principle of the reflection soliton oscillator. The one-port amplifier was implemented using bipolar transistors[7] with maximum unity current gain frequencies of 5 GHz. The NLTL was constructed by forming an LC ladder network with 24 inductor-varactor sections.[8] The procedure to choose the values of the inductors and varactors constituting the NLTL to attain the target repetition frequency and pulsewidth is described in Appendix B. A 6-V dc power supply was used.

The prototype oscillator self-starts from ambient noise, and always reaches a steady state where a stable periodic train of pulses is self-sustained. The oscillation waveforms are measured using an Agilent Infiniium 54855A 6-GHz oscilloscope in conjunction with Agilent 1156A active probes with high impedance (100 kΩ).

Fig. 10 shows a startup transient measured at the open end of the NLTL. As discussed earlier, this signal corresponds to the nonlinear superposition of the incoming and reflected solitons. As the pulse amplitude grows with time, its width is decreased. This amplitude-dependent width is a key soliton property [6], [7]. It is also observed that with the growing pulse amplitude, the pulse repetition rate is increased: e.g., in the figure, $T_1 > T_2$. This is due to another soliton property that a taller soliton propagates faster [6], [7].

Fig. 11(a) shows a stable periodic train of pulses measured at the open end of the NLTL in the steady state, and Fig. 11(b) shows its Fourier transform into the frequency domain, where the Fourier transform is performed using the fast Fourier transform (FFT) capability of the Agilent Infiniium 54855A oscilloscope. The pulsewidth and pulse repetition period are 445 ps and 9.7 ns (4.6% of duty cycle; 103 MHz of pulse repetition rate; many higher harmonics well into the gigahertz frequencies).

Fig. 12 shows measured $V_A(t)$ and $V_B(t)$ from the initial startup to the steady state (V_A, V_B, transistors, and other circuit components mentioned here are with reference to Fig. 8), which is the experimental counterpart of the hypothetical illustration of the same dynamics in Fig. 7. This measurement confirms the machinery of our reflection amplifier described in Section III. First, initially $V_A(t)$ is larger than $V_B(t)$, and thus, $\mathbf{N}_1$ is ON and $\mathrm{Re}\{Z_A\} < 0$, enabling the oscillation startup. Second, as the pulse train is formed and grows, the capacitors in the RC network accumulate more charges, increasing the dc average of $V_B(t)$. Third, in the steady state, the lower portion of $V_A(t)$ goes below $V_B(t)$, turning off $\mathbf{N}_1$, and yielding $\mathrm{Re}\{Z_A\} > 0$. Therefore, the lower portion of $V_A(t)$ is attenuated. In contrast, a higher portion of $V_A(t)$ lies above $V_B(t)$, and thus, $\mathbf{N}_1$ is turned on, and $\mathrm{Re}\{Z_A\} < 0$. Therefore, the higher portion of V_A receives gain. The level-dependent gain is thus properly set up during the steady state, leading to the stable pulse oscillation.

Fig. 13 shows how the pulse shape changes in the steady state as it travels back and forth on the NLTL. At a given time, there is only one pulse traveling on the NLTL. The middle of Fig. 13 shows voltage $V_{16}(t)$ measured at the 16th node on the NLTL,

[7]For npn transistors, Philips BFT25A bipolar transistors were used. For pnp transistors, Philips BFT93 bipolar transistors were used.

[8]For inductors, API Delevan 4426 series air core inductors were used. For varactors, Zetex ZMV930 varactors were used.

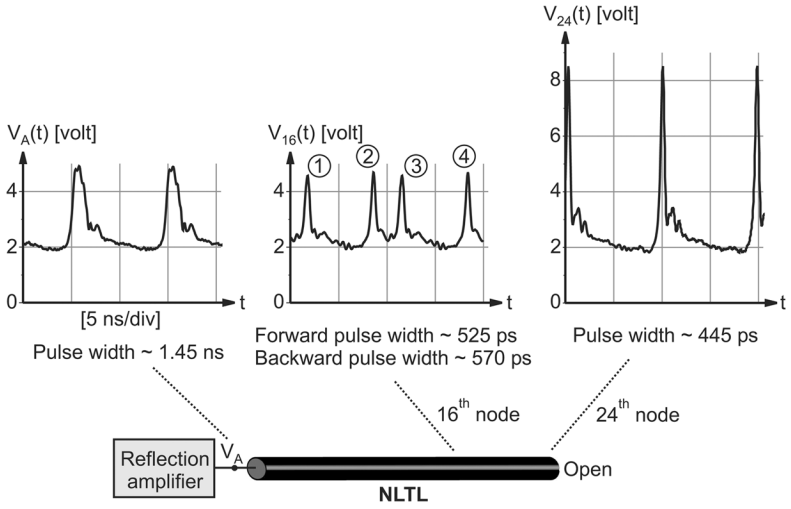

Fig. 13. Measured steady-state oscillation at various points.

where the node number is counted from the amplifier end. Pulse ① propagates backwards (towards the amplifier). This pulse is reflected by the amplifier, and propagates forward (toward the open end), reemerging at the 16th node as pulse ②. This pulse is then reflected at the open end, and travels backwards again, thus reappearing at the 16th node as pulse ③. At the amplifier end (see Fig. 13, left) and at the open end (see Fig. 13, right), the forward and backward waves superpose, and we see their combined effect.

As can be seen in Fig. 13, the pulse at the amplifier end (1.45 ns is the width of the joint pulse; the estimated width of the actual forward pulse without the superposition is 900 ps) is sharpened into a soliton, traveling down the NLTL, leading to a pulsewidth of 525 ps at the 16th node (②, ④). As this soliton reaches the open end, the nonlinear superposition occurring during the reflection (see Section II-B) amplifies the pulse amplitude by 2.4 times and further sharpens the pulsewidth to 445 ps. The backward soliton has lower amplitude and broader width (see ①, ③ in comparison to ②, ④) due to soliton damping [15].

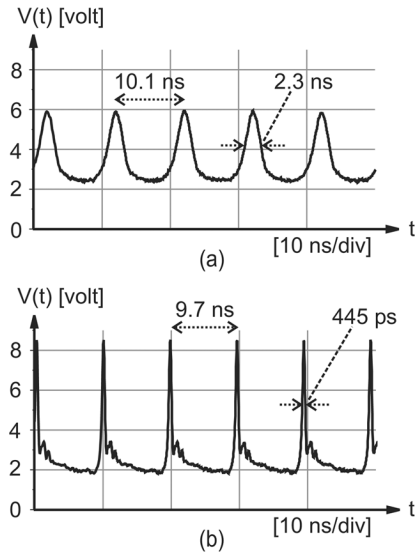

Fig. 14. (a) Measured steady-state oscillation in the Haus oscillator we built. (b) Measured steady-state oscillation in our oscillator: redrawing of Fig. 11(a).

V. Comparison With Haus's Oscillator

As discussed at the beginning of this paper, our reflection soliton oscillator is an alteration of Haus's reflection pulse oscillator [see Fig. 1(b)] [5]. We here compare the two oscillators in terms of circuit design style and pulse-sharpening capability.

Circuit Design: Haus implemented the level-dependent gain using two separate active circuits [see Fig. 1(b)]: an IMPATT diode circuit terminating one end of the linear transmission line produces a nearly constant negative resistance (constant gain); a Schottky diode circuit terminating the other line end executes level-dependent attenuation. Their combined effect is the level-dependent gain. The adaptive bias scheme was incorporated in the Schottky diode circuit. In contrast, in our oscillator (see Fig. 8), the level-dependent gain and the adaptive bias scheme are all incorporated in a single one-port amplifier using bipolar transistors, which terminates one end of the NLTL (the other end of the NLTL is open).

Pulse Sharpening: In Haus's oscillator, pulse sharpening is provided only through the level-dependent gain, and thus, it is limited by the bandwidth of the active circuits providing the level-dependent gain. In our oscillator, the dominant pulse-sharpening mechanism is provided by the NLTL. Since the NLTL's pulse sharpening (see Fig. 13) is not limited by the bandwidth of the reflection amplifier, our oscillator has an improved pulse-sharpening ability. To experimentally show this improvement, we constructed a Haus oscillator by replacing varactors in our NLTL with linear capacitors. Fig. 14(a) is the measured steady-state signal at the open end of the linear line in the Haus oscillator we constructed, while Fig. 14(b) [redrawing of Fig. 11(a)] is the measured steady-state signal at the open end in our oscillator. Our reflection soliton oscillator achieves a five times sharper pulsewidth.

VI. Comparison With Circular Soliton Oscillator

The design spirit of our reflection soliton oscillator, and its utilization of the level-dependent gain for soliton oscillation stabilization, originate from our earlier work on the circular soliton oscillator (see Fig. 1(c), [6] and [7]). We compare the two oscillators' performance and design merits.

Energy Efficiency: In the circular soliton oscillator, the energy of a circulating pulse is dissipated in a termination network at the input of the two-port amplifier to prevent a reflection. It is the voltage of the circulating pulse that is sensed and amplified by the amplifier to recreate a pulsed energy at the output of the amplifier. This energy dissipation and recreation at each cycle of pulse circulation corresponds to an energetically inefficient operation. In contrast, in the reflection soliton oscillator, the one-port amplifier *pushes back* the oncoming pulse energy, while adding some energy to compensate for loss, and thus, energy is recycled with no intentional energy dissipation. Overall, the reflection soliton oscillator utilizes energy more efficiently.

Pulsewidth: As discussed in Section II-B, the reflection at the open end of the NLTL in the reflection soliton oscillator sharpens the pulse at that end. This is an extra sharpening mechanism, in addition to the pulse sharpening that occurs during the propagation on the NLTL. Such a reflection-mediated pulse sharpening does not exist in the circular soliton oscillator, and thus, the reflection soliton oscillator can potentially achieve a narrower pulsewidth.

Circuit Size: To achieve a pulse repetition rate of f for a pulse propagation speed of v, the reflection soliton oscillator requires an NLTL length of approximately $v/(2f)$, while the circular soliton oscillator requires a twice longer NLTL length (v/f) (these are approximations because delays caused by amplifiers will somewhat affect the pulse repetition rate). Given that the NLTL is by far the largest part of both circuits, the reflection soliton oscillator will have an almost twice smaller physical size than the circular soliton oscillator.

VII. Conclusion and Future Work

Cutler (1955) established the principle of electrical pulse oscillators by constructing a circular pulse oscillator. Haus (1978) altered the design to construct a reflection pulse oscillator. Both Cutler and Haus's oscillators use linear pulse propagation media while pulse formation/sharpening is executed by lumped amplifiers. If pulse sharpening can occur in its propagation medium, the pulse oscillator can generate much sharper pulses, thus enriching the scope and capacity of electrical pulse oscillators. This paper reported on one such oscillator, where we replaced the linear pulse propagation medium in Haus's reflection pulse oscillator with an NLTL, which has been long known for its pulse compression ability. A specially designed one-port reflection amplifier at one end of the NLTL stabilizes the oscillation, by taming the inherently unruly pulse dynamics on the NLTL. The oscillator self-generated a stable train of sharp soliton pulses. This work is a counterpart of our earlier work (see [6] and [7]) where we made a similar nonlinear transition from Cutler's circular pulse oscillator.

The reflection soliton oscillator prototype reported in this paper was at a discrete level, and its signal occupied the lower end of the microwave spectral range. We deliberately chose the relatively slower operation speed in order to facilitate real-time measurements of the oscillator signal, and thus to fully verify the operating principle of the reflection soliton oscillator. Now with the essential operating principle firmly demonstrated, the reflection soliton oscillator, especially its NLTL, can be scaled to a smaller size on an integrated circuit to substantially increase the operation speed. For instance, GaAs NLTLs capable of generating picosecond or sub-picosecond pulses [10], [17] can be used in an integrated GaAs reflection soliton oscillator to significantly reduce the soliton pulsewidth. Although the amplifier even in the state-of-the-art GaAs technology cannot provide gain for such short-duration pulses, it might be possible that the pulse sharpening on the NLTL can overcome the bandwidth limitation. Demonstration of such an ultrafast reflection soliton oscillator is open to future studies.

Appendix A
Proof of (3)

In the NLTL consisting of inductor-varactor sections (see Fig. 4), if loss is ignored (this is justifiable, as the quality factor of our NLTL is around 100 in the operation frequency range), the following holds for any n according to Kirchhoff's Voltage Law (KVL):

$$L\frac{\partial I_{n+1}(t)}{\partial t} = V_n(t) - V_{n+1}(t).$$

The time integration of the left-hand side from $t = -\infty$ to ∞ reduces to zero, as pulses die down at $t = \infty$ and do not exist $t = -\infty$. Therefore, the time integration of the right-hand side from $t = -\infty$ to ∞ is zero, or

$$\int_{-\infty}^{\infty} V_n(t)dt = \int_{-\infty}^{\infty} V_{n+1}(t)dt \quad \text{(for any } n\text{)}.$$

This is equivalent to (3). *QED*.

Appendix B
NLTL Design Procedure

Here we describe how we chose the values of inductors and varactors of the NLTL of N LC sections in our discrete prototype to obtain target pulse repetition rate and pulsewidth. First, in a lossless NLTL, the temporal soliton width W is approximated as [16]

$$W \approx \frac{3 - 2bA}{\sqrt{6bA}}\sqrt{LC_0} \tag{4}$$

where A is the soliton amplitude, $C(v) = C_0(1 - 2bv)$ is the varactor capacitance as a function of applied voltage v, and L is

the inductance. Second, the pulse repetition rate of the reflection soliton oscillator is [16]

$$f = \frac{1}{2N\Delta + \tau_{\rm amp}} \tag{5}$$

where Δ is a propagation delay through a unit inductor-varactor network, which is approximated as

$$\Delta \approx \sqrt{\frac{3-2bA}{3}}\sqrt{LC_0}$$

in the absence of loss, and $\tau_{\rm amp}$ is the delay caused by the reflection amplifier. For target values of f and W, we have enough degrees of freedom to choose component values that satisfy (4) and (5), and thus, these equations are useful as initial design guidelines.

In the final stage of design after starting with the equation-based component selection, we resorted to circuit simulations to finalize the component values for the following reasons. First, W and f are functions of not only the component values, but also the soliton amplitude A, which is difficult to express in terms of component values. Second, the equations above assume that the pulse waveform is the same everywhere on the NLTL in steady-state oscillation, while this is untrue, as seen in Section IV. Third, both the varactor model $C(v) = C_0(1-2bv)$ and zero loss assumption used to obtain equations above are approximate.

ACKNOWLEDGMENT

The authors thank N. Sun and D. Ha, both with Harvard University, Cambridge, MA, for their valuable feedback, and Sonnet Software, North Syracuse, NY, and the Ansoft Corporation, Pittsburgh, PA, for their donated electromagnetic (EM) field solvers, and Agilent EEsof EDA, Santa Clara, CA, for their donated Advanced Design System (ADS) software.

REFERENCES

[1] M. Kahrs, "50 years of RF and microwave sampling," *IEEE Trans. Microw. Theory Tech.*, vol. 51, no. 6, pp. 1787–1805, Jun. 2003.

[2] R. Y. Yu, M. Reddy, J. Pusl, S. T. Allen, M. Case, and M. J. W. Rodwell, "Millimeter-wave on-wafer waveform and network measurements using active probes," *IEEE Trans. Microw. Theory Tech.*, vol. 43, no. 4, pp. 721–729, Apr. 1995.

[3] G. F. Ross, "Transmission and reception system for generating and receiving base-band pulse duration pulse signals without distortion for short base-band communication system," U.S. Patent 3 728 632, Apr. 17, 1973.

[4] C. C. Cutler, "The regenerative pulse generator," *Proc. IRE*, vol. 43, no. 2, pp. 140–148, Feb. 1955.

[5] L. A. Glasser and H. A. Haus, "Microwave mode locking at X-band using solid-state devices," *IEEE Trans. Microw. Theory Tech.*, vol. MTT-26, no. 2, pp. 62–69, Feb. 1978.

[6] D. Ricketts, X. Li, and D. Ham, "Electrical soliton oscillator," *IEEE Trans. Microw. Theory. Tech.*, vol. 54, no. 1, pp. 373–382, Jan. 2006.

[7] D. Ricketts, X. Li, N. Sun, K. Woo, and D. Ham, "On the self-generation of electrical soliton pulses," *IEEE J. Solid-State Circuits*, vol. 42, no. 8, pp. 1657–1668, Aug. 2007.

[8] R. Landauer, "Shock waves in nonlinear transmission lines and their effect on parametric amplification," *IBM J. Res. Develop.*, vol. 4, no. 4, pp. 391–401, Oct. 1960.

[9] R. Hirota and K. Suzuki, "Theoretical and experimental studies of lattice solitons in nonlinear lumped networks," *Proc. IEEE*, vol. 61, no. 10, pp. 1483–1491, Oct. 1973.

[10] M. Rodwell *et al.*, "Active and nonlinear wave propagation devices in ultrafast electronics and optoelectronics," *Proc. IEEE*, vol. 82, no. 7, pp. 1037–1059, Jul. 1994.

[11] M. Case, M. Kamegawa, R. Y. Yu, M. J. W. Rodwell, and J. Franklin, "Impulse compression using soliton effects in a monolithic GaAs circuit," *Appl. Phys. Lett.*, vol. 68, no. 2, pp. 173–175, Jan. 14, 1991.

[12] M. Tan, C. Y. Su, and W. J. Anklam, "7× electrical pulse compression on an inhomogeneous nonlinear transmission line," *Electron. Lett.*, vol. 24, no. 4, pp. 213–215, Feb. 1988.

[13] M. Remoissenet, *Waves Called Solitons: Concepts and Experiments*. New York: Springer, 1999.

[14] M. Toda, *Nonlinear Waves and Solitons*. Norwell, MA: Kluwer, 1989.

[15] E. Ott and R. N. Sudan, "Damping of solitary waves," *Phys. Fluids*, vol. 13, no. 6, pp. 1432–1434, June 1970.

[16] D. Ricketts, "The electrical soliton oscillator," Ph.D. dissertation, School Eng. Appl. Sci., Harvard Univ., Cambridge, MA, 2006.

[17] D. W. van der Weide, "Delta-doped Schottky diode nonlinear transmission lines for 480-fs, 3.5-V transients," *Appl. Phy. Lett.*, vol. 65, no. 7, pp. 881–883, Aug. 1994.

O. Ozgur Yildirim (S'08) received the B.S. and M.S. degrees in electrical and electronics engineering from Middle East Technical University (METU), Ankara, Turkey, in 2004 and 2006, respectively, and is currently working toward the Ph.D. degree in electrical engineering and applied physics at Harvard University, Cambridge, MA.

In the summers of 2002 and 2003, he was with the Scientific and Research Council of Turkey (TUBITAK), Ankara, Turkey, where he was involved with a dynamic power compensation card and a field-programmable gate array (FPGA) for synchronous dynamic RAM interface, respectively. While earning the master's degree, he was involved with the development of on-chip readout electronics for uncooled microbolometer detector arrays for infrared camera applications. His research interests include RF, analog, and mixed-signal integrated circuits, soliton and nonlinear wave phenomena and their utilization in electronic circuits, and terahertz electronics.

Mr. Yildirim was the recipient of the 2009 Analog Devices Outstanding Student Designer Award.

David S. Ricketts (S'98–M'06) received the Ph.D. degree in electrical engineering from Harvard University, Cambrige, MA, in 2006

He then joined the faculty of Carnegie Mellon University, Pittsburgh, PA, where he is currently an Assistant Professor with the Electrical and Computer Engineering Department. He possesses 12 years industrial experience in the development of over 40 integrated circuits in mixed-signal, RF, and power management applications. His research crosses the fields of device physics, material science, physics, and circuit design, investigating the ultimate capabilities of microelectronic devices, and how these are harnessed by differing circuit topologies to produce the highest performing systems. His research has appeared in *Nature* and in numerous IEEE conferences and journals and was selected for the 2008 *McGraw Hill Yearbook of Science and Engineering*. He coauthored *The Designer's Guide to Jitter in Ring Oscillators* (Springer, 2009).

Prof. Ricketts was a Harvard Innovation Fellow and Wimmer Faculty Teaching Fellow. He was the recipient of the Defense Advanced Research Projects Agency (DARPA) Young Faculty Award and the George Tallman Ladd Research Award.

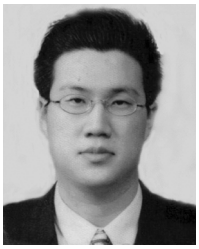

Donhee Ham (S'99–M'02) received the B.S. degree (*summa cum laude*) in physics from Seoul National University, Seoul, Korea, in 1996, and the Ph.D. degree in electrical engineering from the California Institute of Technology, Pasadena, in 2002. His doctoral dissertation concerned the statistical physics of electrical circuits.

He is a Gordon McKay Professor of Electrical Engineering and Applied Physics with Harvard University, Cambridge, MA, where he is with the School of Engineering and Applied Sciences. Following one and one-half years of mandatory military service in Korea Army, he joined the Physics Department, California Institute of Technology, where he spent the first two years involved with general relativity and gravitational astrophysics. His professional experience also includes the California Institute of Technology–Massachusetts Institute of Technology (MIT) Laser Interferometer Gravitational Wave Observatory (LIGO) and the IBM T. J. Watson Research Center. He was a coeditor of *CMOS Biotechnology* (Springer, 2007). His research at Harvard University has focused on quantum plasmonics with 1-D conductors, applications of CMOS integrated circuits (ICs) in biotechnology, soliton and nonlinear wave electronics, spin-based quantum computing on silicon, statistical thermodynamics of electronic circuits, and RF/microwave, analog, and mixed-signal integrated circuits.

Dr. Ham has been a member of IEEE conference technical program committees including the IEEE International Solid-State Circuits Conference (ISSCC) and the IEEE Asian Solid-State Circuits Conference (ASSCC). He has been on the Advisory Board for the IEEE International Symposium on Circuits and Systems (ISCAS), International Advisory Board for the Institute for Nanodevices and Biosystems, and various U.S., Korea, and Japan industry, government, and academic technical advisory positions on subjects including ultrafast electronics, science and technology at the nanoscale level, and the interface between biotechnology and solid-state circuits. He was a guest editor for the IEEE JOURNAL OF SOLID-STATE CIRCUITS (January 2009). He was the recipient of the Valedictorian Prize, as well as the Presidential Prize, ranked top first across the Natural Science College, and also the Physics Gold Medal (sole winner). He was the recipient of the Charles Wilts Doctoral Thesis Prize, Best Thesis Award in Electrical Engineering. He was the recipient of the IBM Doctoral Fellowship, IBM Faculty Partnership Award, IBM Research Design Challenge Award, Li Ming Scholarship, and Silver Medal in National Mathematics Olympiad. He was the Fellow of the Korea Foundation of Advanced Studies. He was a corecipient of the Harvard Hoopes Prize. He was recognized by *MIT Technology Review* as among the world's top 35 young innovators in 2008 (TR35) for his group's research on CMOS RF biomolecular sensor using nuclear spin resonance to pursue early disease detection and low-cost medicine.